An imaging system for accurate target positioning for fast focusing geometries

Contact *david.carroll@strath.ac.uk*

D.C. Carroll and P. McKenna

Department of physics, University of Strathclyde, SUPA, Glasgow G4 0NG, UK

S. Kar and M. Borghesi

School of Mathematics and Physics, Queen's University Belfast, Belfast BT7 1NN

P. Foster, D. Symes, R. Pattathil and D. Neely

[*]Central Laser Facility, STFC RAL, Oxfordshire OX11 0QX, UK

Introduction

For the first time, an F/0.87 on-axis parabolic mirror was fielded on a recent experiment on the Astra-Gemini laser. The purpose of using this optic was to achieve higher laser intensity with a smaller focal spot compared to that typically achieved with the F/2 off-axis parabolic mirror (OAP) used in previous solid target experiments. Positioning of targets relative to the tight focus of the laser for an F/2 OAP has been achieved using a retro-focusing system. It has been shown previously that the current retro system is at the limit of its capability with the F/2 in terms of reliably positioning the target [1] and with the F/0.87 parabola the required accuracy of positioning is higher due to the shorter Rayleigh range.

In this report we describe an imaging system implemented in recent experiments to achieve the required positioning accuracy needed, when using an F/0.87 focusing optics.

Motivation

The Rayleigh range, z_R, over which the intensity of the laser is reduced by a factor of √2 defines the upper limit of the accuracy to which a target alignment system must achieve during target positioning. The Rayleigh range is related to the beam waist size, w_0, at its narrowest point defined where the signal drops to $1/e^2$. For a Gaussian beam this is related to the FWHM spot size by $w_0 = 0.85d_{G,FWHM}$ and for a super Gaussian beam by $w_0 = 0.65d_{S,FWHM}$.Where λ is the laser wavelength, the Rayleigh range is defined as:

$$z_R = \frac{\pi w_0^2}{\lambda}$$

For the F/2 parabola where a focal spot of 2.5 µm (FWHM) is achieved, the Rayleigh range is 10.4 µm for the super Gaussian Gemini beam. The current target alignment system in Gemini is a retro-imaging system with accuracy of positioning the target that is at this limit [1]. For the F/0.87 parabola a focal spot of 1.0 µm has been measured which gives a Rayleigh range for a super Gaussian of 1.7 µm. This is beyond the capability of the current retro imaging system and so requires a different system for positioning the target.

Parabola	Spot size (FWHM, µm)	z_R Gaussian (µm)	z_R super Gaussian (µm)
F/2	2.5	17.7	10.4
F/0.87	1.0	2.8	1.7

Table. 1: The Rayleigh ranges for the F/2 and F/0.87 parabolic mirrors based on the measured spot sizes for λ = 800 nm.

New imaging system

The imaging system implemented to achieve the required accuracy was a camera with a high power objective mounted on a xyz translation stage which allowed it to be driven into position to image the laser spot between shots. An image of this setup is shown in Figure 1. The alignment procedure is to drive the camera in and adjust its position until the laser focal spot imaged by the camera is at best focus. The target is then driven in and the target rear surface is brought into focus on the camera which is still imaging the point of best focus. For very thin, sub-micron, targets this ensures the laser focal spot and the target surface plane are equivalent. For thicker targets a correction for the target thickness is required to ensure the target front surface is at the best focus of the laser. For very thin targets the surface quality is mirror like and so bringing into focus is achieved by imaging dust particles on the target surface.

The main imaging objective used is a 100X Mitutoyo Plan Apo NIR HR Infinity-Corrected Objective. This objective has a numerical aperture of 0.7 which gives an equivalent f-number of F/0.71 which is sufficient to image the F/0.87 parabola focal spot. The resolving power and depth of focus of the objective are 0.39 µm and 0.56 µm respectively and so enable resolution of the 1.0 µm focal spot. Another important consideration for the objective is the working distance, defined as how far from the focal spot the objective is when it is aligned. A simple x60 microscope objective is able to resolve the focal spot but has a working distance of ~0.3 mm which leaves minimal distance to avoid collisions with the target and any mount that is holding the target. The Mitutoyo objective has a 10.0 mm working distance which provides a much larger safety margin. A schematic of the setup is shown in Figure 2.

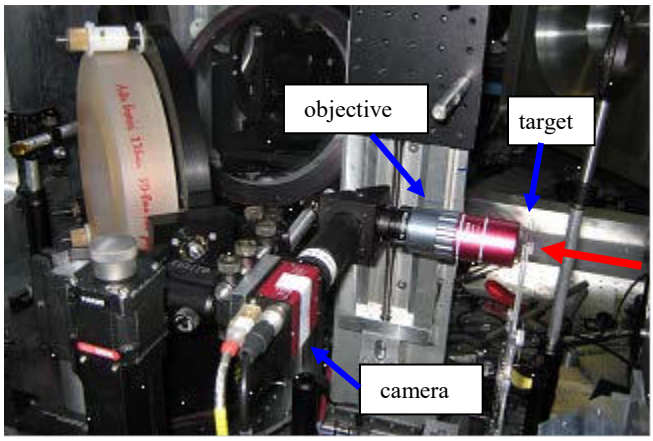

Figure 1: Alignment camera with objective *in situ* imaging a target. The red arrow indicates the direction of the laser off the F/0.87 parabola.

Additionally, when using the F/0.87 parabola the on-axis focusing must be taken into consideration. This means that the

camera-objective setup will block part of the incoming beam. This necessitates a minimal camera profile where possible.

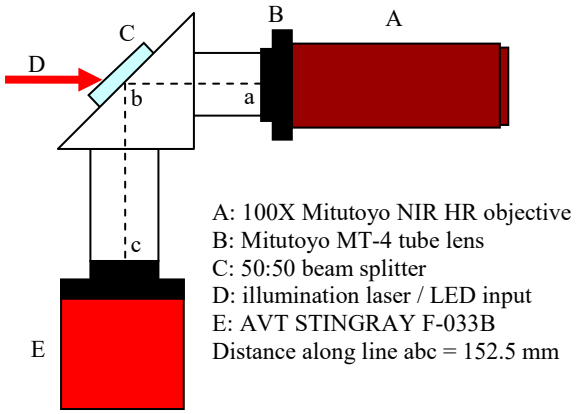

Figure 2: Schematic of alignment camera set-up. Have the turn with beam splitter enables a separate illumination source to be injective through the back of the objective and ensures the minimum profile in the main beam line by keeping the camera out of the beam line.

Illumination

To align the target to the parabola focus the target rear surface is brought into focus on the imaging camera. To ensure there is sufficient light for the camera to image the rear surface of the target a separate light source is used. To avoid errors in positioning this light source is the same wavelength as the main laser beam, $\lambda = 800$ nm.

Two different light sources were tested; a CW laser diode and an 800 nm LED. Both light sources were injected by the same method through the back of the objective via a beam splitter. Though we found that alignment could be done with either laser or LED illumination we found that the LED was more suitable due to being easier to set-up (by simply placing the LED directly behind the beam splitter, no beam line is required) and providing a much better illumination of the target surface, as shown in Figure 3. With the laser we found that internal reflections in the imaging system resulted in laser light being focused onto the camera chip. This focussed light was not imaged from the target surface and obscured the real image. Adding a glass diffuser to scatter the laser light did not improve the imaging.

Advantages and disadvantages

Target alignment with a high resolution objective-camera setup has several advantages over a retro imaging system. Firstly, you are able to monitor the focal spot during a sequence of laser shots. Secondly, there is no requirement of matching a separate alignment laser to the main laser and thirdly it enables the user to check for damage to the target and its quality *in situ*. However, there are a number of drawbacks with the system. These are a longer alignment time for each target due to having to drive the camera in and out every time and the camera being *in situ*. Where the retro imaging alignment can achieve a reasonable shot rate of every 5 minutes, for the camera-objective imaging with an LED illumination this is 15-20 minutes and for very high quality targets with a mirror finish and minimal surface dust to focus on it can take longer. A second draw back is that the camera is *in situ* and so takes up valuable space around the interaction region. Furthermore, a portion of the incoming laser beam will be blocked when using the objective-camera setup in the on-axis parabola configuration.

Conclusion

An alignment system consisting of a camera with a high power imaging objective was implemented to enable a high level of accuracy in aligning thin foil targets when the main focusing optic is an F/0.87 parabolic mirror with a very short Rayleigh range. This was found to be successful but at the cost of a slower shot rate.

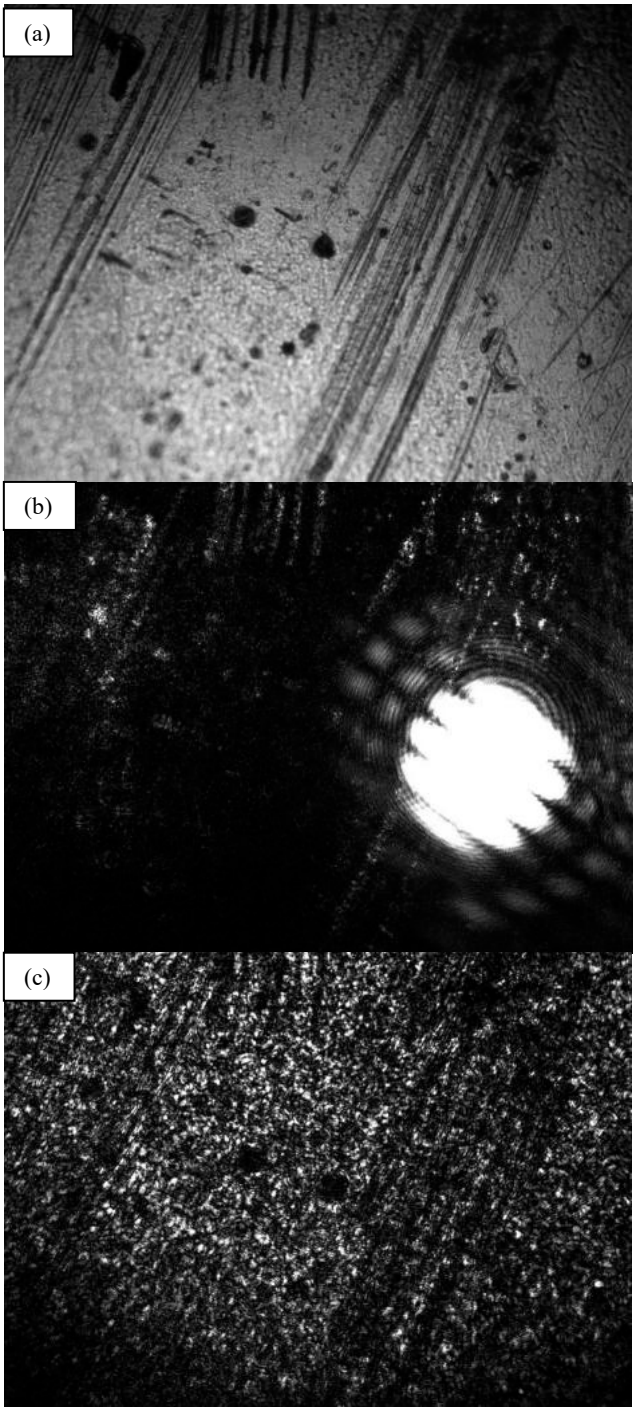

Figure 3: Target surface imaged with an objective where the illumination is provided through the back of the objective. (a) illumination provided by an LED. (b) illumination provided by a CW diode laser. (c) illumination provided by the same laser as in (b) but with a glass diffuser to scatter the light.

Acknowledgements

We acknowledge the expert support provided by the staff at the Central Laser Facility of the Rutherford Appleton Laboratory.

References

1. D. Carroll *et al.* “An assessment of the reproducibility of the Gemini retro focusing system” CLF annual report 2010/2011.

Implementation of Pulse Measurements with Wizzler into Gemini Diagnostics.

Contact *Oleg.Chekhlov@stfc.ac.uk*

O. Chekhlov, C. Hooker, S. Hawkes, V. Marshal, B. Parry, Y. Tang and R. Pattathil

Central Laser Facility,
STFC Rutherford Appleton Laboratory, Harwell-Oxford, Oxon OX11 0QX, UK

The arsenal of devices for measuring ultrashort light pulses has been recently reinforced by a device for spectral phase measurement known as a "Wizzler"®. The Gemini laser diagnostics have benefitted from the acquisition of a Wizzler and an upgrade of our Dazzler. Here we present some results of their application to the Gemini laser pulses.

The reliability of measurements of femtosecond laser pulses is always under scrutiny particularly for those cases when spectral phase of the pulse is retrieved near the edges of the pulse spectrum. This is especially true for pulse measuring devices such as FROG or SPIDER based on measuring light at its second harmonics. Devices which use other nonlinear effects such as self-phase modulation and spectral broadening are thought to be more reliable in measuring spectral phase at the bottom of the pulse spectral width. The Wizzler device, which is a commercially available from Fastlite (France) [1], measures the pulse parameters using spectral interferometry [2] of the test optical pulse with a reference pulse with a flat spectral phase. This reference pulse is collinearly generated from the input pulse by cross polarized wave generation (XPW). A non integrative processing of the spectral interference pattern resulting from the combination of the input pulse and the reference pulse allows for direct retrieval of the spectral phase and intensity of the pulse.

One of the attractive features of the Wizzler is that it is easy to establish a feedback link to the Dazzler, which is an acousto-optical filter used in the Astra Gemini kHz preamplifier for spectral phase and amplitude control. The feedback link was established via the Gemini laser computer network connection. The feedback phase file helps to modify the spectral phase of the optical pulse, aiming to achieve a flat spectral phase in order to minimize the pulse duration after compression.

The measurements were made using the pulse diagnostic beam which is transmitted through a hole in the last mirror of the compressor. The 5 Hz pulse train from Astra was used, with around 1.5 mJ per pulse in the test beam. The effect of feedback application to the Dazzler can be seen from comparison of Figures 1 and 2. The spectral phase in Fig.1 was measured on the North beam with only polynomial phase correction applied to the Dazzler and with phase correction from the file switched off. The feedback link allows an easy modification of previous phase file with subsequent corrections. Several iterative steps of correction were made to optimize the feedback strength and wavelength offset between Dazzler and Wizzler. The red line in Fig.2 represents the measured spectral phase of the pulse after phase correction. The pulse duration was 40 fs, which corresponds to a transform limited pulse with spectral bandwidth of 35.9 nm and measured spectral shape given by the white line in Fig.2.

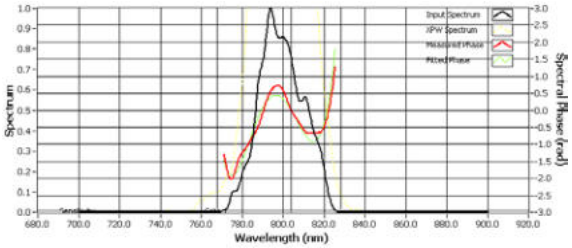

Figure 1. Spectral phase (red line) of the North beam measured with the Wizzler pulse measuring device together with input spectrum (black line).

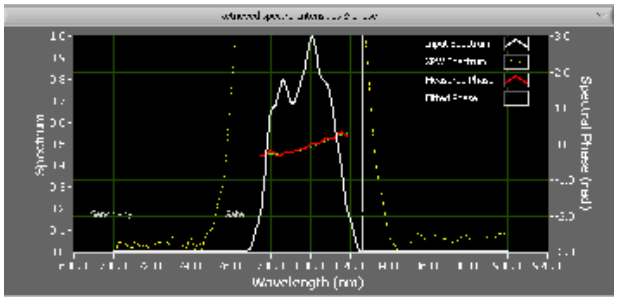

Figure 2. Measured spectral phase (red line), input spectrum (white line) and XPW spectrum (dashes) of Gemini pulse after correcting the phase.

The essential part of the implementation of the Wizzler–Dazzler spectral phase monitor and control was the upgrade of the WB-800/T2 Dazzler system to a jitter free HR-800/T3 model. The newer model has 0.3nm resolution and maximum programmable delay of 8ps. Direct application of the measured phase from the Wizzler device still caused substantial change of RF signal on Dazzler, as can be seen from Figure 3. The change in amplitude of the signal was caused mainly by the fourth order term, which decreased the Dazzler efficiency. This was mitigated by modifying the shape of the correcting phase close to the edges of the spectral window of the phase file.

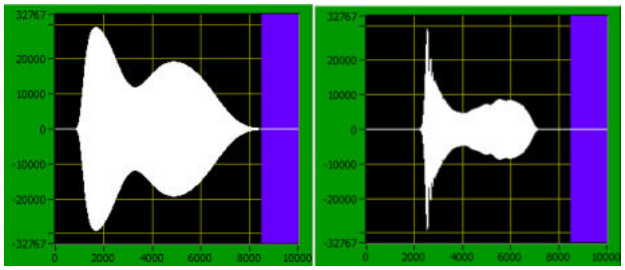

Figure 3. The shapes of RF signal applied to Dazzler crystal without phase file (left) and with the phase file(right).

We have recently installed a Wizzler device for measuring the temporal parameters of the laser pulses in the Gemini laser system and upgraded the Dazzler at the front end of Astra. The spectral phase correction applied via a feedback link between two devices provides a fast way to apply spectral phase corrections and achieve transform-limited pulses.

References

1. http://www.fastlite.com/en/pag26-WIZZLER.html
2. T. Oksenhendler, S. Coudreau, N. Forget, V. Crozatier, S. Grabielle, R. Herzog, O. Gobert, and D. Kaplan, Appl. Phys.B 99, 7 (2010).

Recommissioning of the Pulse Compressor for Astra Target Area 2.

Contact *Oleg.Chekhlov@stfc.ac.uk*

O. Chekhlov, C. Hooker, D. Symes, S. Tomlinson, A. Zayyani, D. Rathbone, S. Hawkes, V. Marshal, B. Parry, Y. Tang and R. Pattathil

Central Laser Facility,
STFC Rutherford Appleton Laboratory, Harwell-Oxford, Oxon OX11 0QX, UK

Introduction

The multi-terawatt target area of the Astra laser system (ATA2) [1], which was out of operation for several years, has recently been upgraded with new control systems for vacuum, interlocks and motion control. The aim of these upgrades was to bring ATA2 back into operation with the same standards of controls as elsewhere in the CLF. As part of the upgrade we installed a newly-designed mount for the second grating of the pulse compressor. Here we report on the recommissioning of the pulse compressor with the new grating mount.

Design of the G2 grating mount

The grating mount for the large grating (G2) of the pulse compressor was redesigned to provide reliable motion control and long term mechanical stability between alignment sessions. A sketch of the grating mount is presented in Figure 1. The mount was designed to accommodate the existing grating of size 333x100x45mm. The grating mount for a pulse compressor should provide 3-axis rotation of the grating to achieve alignment to an accuracy better than the diffraction-limited spot radius. The mount was designed to use stepper motors for driving the axes' rotation. The high resolution of axis rotation was achieved through a combination of worm-wheel gears and gears for the stepper motors. The total gear ratio for groove rotation and tilt rotations is 1:812.5, and 1:350 for diffraction angle rotation. Further precise control of the mount rotation steps is achieved through changeable ratios in the software setup of the drive system. The grating mount is located on a linear translation stage driven by a stepper motor. All positioning references are managed through the drive system control software: there is no independent readout of the length position of the grating.

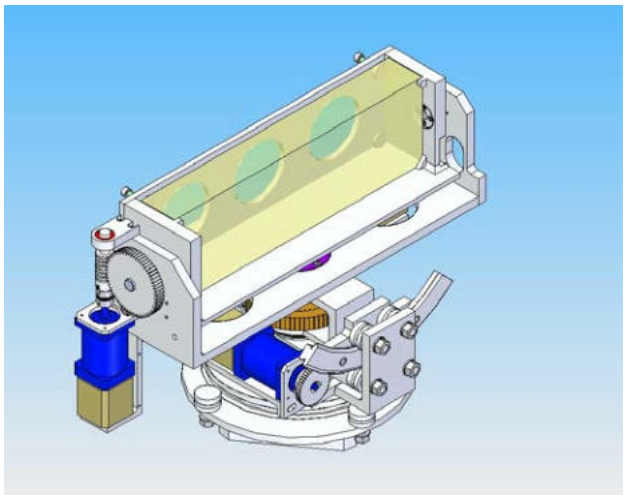

Figure 1. Three dimensional view of the mount design for the second grating of the pulse compressor in ATA 2.

Pulse compressor alignment and pulse measurement.

The pulse compressor has a double pass design with two reflective diffraction gratings (1480 lines/mm) and a single back reflective mirror. The input and output beams are separated thanks to a ~1.5 degree tilt of the input beam relative to the plane of diffraction angle. The compressor length is adjusted to compress a 500ps stretched pulse. The compression of the pulse is monitored by measuring the pulse duration of a portion of the output beam which passes through a small hole in the turning mirror for the output beam. The diagnostic beam is taken out from the compressor chamber through thin window with negligible second order dispersion.

The optimization of the compressor was performed by measuring the pulse duration and spatial properties of the focused beam. The pulse measurements were carried out using LX-SPIDER® from APE GmbH (Germany) [2]. The pulse measuring technique of LX -SPIDER is based on spectral shearing interferometry. Typical measured spectral phase and pulse shape are presented in Figure 2.

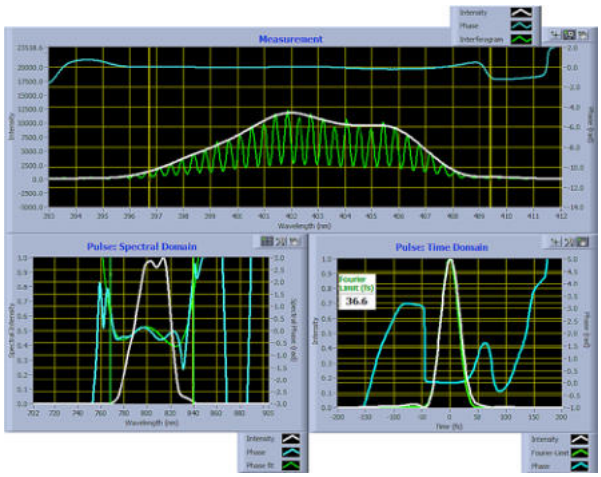

Figure 2. The compressed pulse parameters measured by LX-SPIDER: Top plot: spectral interferogram of the second harmonics (green); bottom left: spectral phase dependence (blue); bottom right: pulse shape (white) and temporal phase (blue).

The pulse duration in Figure 2 corresponds to 39 fs which was achieved purely by compressor alignment without making fine phase file correction with Dazzler device.

Conclusions

The recommissioning of the pulse compressor in ATA2 has been successful. The temporal pulse parameters were close to transform limited. The ATA2 compressor has been handed over to the user group s experiment.

References

1. A J Langley, E J Divall, C H Hooker, M H R Hutchinson, A J-M P Lecot, D Marshall, M E Payne, P F Taday "The Development of a Multi-Terawatt Femtosecond Laser Facility – Astra" CLF Ann.Report1999-2000, p.196-200.
2. S.-P. Gorza, A. S. Radunsky, P. Wasylczyk, and I. A. Walmsley "Tailoring the phase-matching function for ultrashort pulse characterization by spectral shearing interferometry", ,J. Opt. Soc. Am. B, 24,(2007), 2064-2074.

Monte Carlo studies of ion-ion inverse Bremsstrahlung absorption

Contact *a.turrell09@imperial.ac.uk*

A. Turrell, M. Sherlock, S. Rose

Blackett Laboratory, Imperial College London
SW7 2AZ

Introduction

A 0D Monte Carlo (MC) code has been developed to study ion-ion inverse Bremsstrahlung absorption in the presence of a linearly polarised laser field in the relativistic to 'ultra-relativistic' regime in which the Lorentz factor of the electrons is much greater than 1. The mechanism is analogous to electron-ion inverse Bremsstrahlung absorption, and applies to two or more species of ion with non-identical charge-to-mass ratios. The effect is increased for increasing densities and increasing Z, or for larger differences in charge-to-mass ratio.

Lasers with intensities of the order of 10^{22} W/cm^2 [1] have been demonstrated and the next generation, including ELI and Vulcan 10PW, will provide intensities reaching 10^{23} W/cm^2, corresponding to the ultra-relativistic regime. New physics is important in this regime, including quantum corrections, pair-production and new absorption processes ([2, 3, 4]).

The interplay of QED-plasma processes in this regime means a full simulation is extremely complex. Rather than solving the full problem, the code models ion-ion inverse Bremsstrahlung absorption in isolation, using an 'effective' intensity, defined as the intensity felt by the ions once other absorption effects are taken into account. As electrons are strongly affected by QED processes in this regime, and are an order of magnitude less effective in the transfer of energy to ions than are other ions, they are ignored. For this reason, only time periods of the order of the ion-ion equilibration time are considered.

The Monte Carlo code

The code is based on Takizuka and Abe's scheme [5]. The distribution of scattering angles for collisions between charged particles i and j is assumed to satisfy $\sim\mathcal{N}(0,\langle\ ^2\rangle)$ where the variance is

$$\langle\ ^2\rangle = \left(\frac{e^2 Z_i Z_j}{4\ \ _0}\right)^2 \frac{n}{2m_{ij}^2 v_{ij}^3}\ \ t \ln\ \ _{ij}$$

with n the lower of the densities of i and j, and t the timestep. Angles for individual collisions are given by a Box-Muller transform [6],

$$\theta = \sqrt{-2\langle\ ^2\rangle \ln U_1}\cos(2\ \ U_2);\ \ U_1, U_2\ \ (0,1]$$

with U_1, U_2 randomly distributed. Energy and momentum are conserved in each collision, and macroscopic variables such as temperature and Coulomb logarithm are updated each timestep.

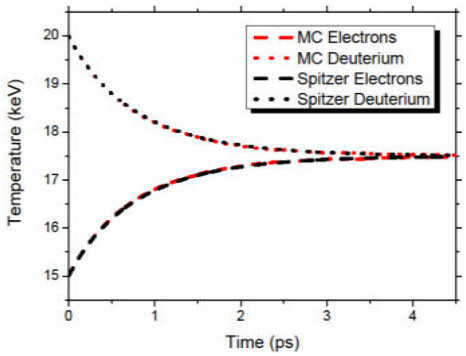

Fig. 1: Electron-ion equilibration for $n_e = n_i = 4\cdot10^{32}$ m^{-3}

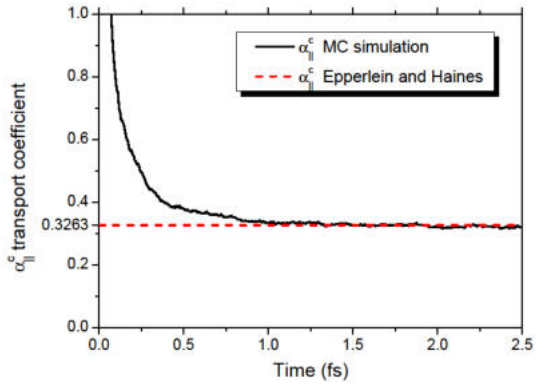

Fig. 2: Electrical resistivity transport coefficient for $\mathbf{B} = \mathbf{0}$, $E_x = 5\cdot10^9$ V/m, Z = 12

The code has been benchmarked against the Spitzer model of temperature equilibration as shown in Fig. 1 and it reproduces the electrical resistivity transport coefficient of Epperlein and Haines [6], Fig. 2.

The laser field

A laser field of period ω propagates in the z-direction, giving all charged particles a forced velocity. It is assumed that the reservoir of laser energy is infinite, and that all particles are fully ionised. The electric field acceleration induces a time-dependent relative velocity between species of different charge-to-mass ratios of

$$\boldsymbol{v} = \frac{e\boldsymbol{E}}{\omega}\cos(\omega t)\left(\frac{Z_i}{m_i} - \frac{Z_j}{m_j}\right)$$

The timestep must resolve ion-ion collisions but is also restricted by the uncertainty in the final momentum of the ions of $\approx Ze\langle\boldsymbol{E}\rangle\Delta t/\omega$. The laser pulse has a Gaussian growth and decay profile.

Ion-ion inverse Bremsstrahlung absorption

Under the guise of driven collisional ion heating, ion-ion inverse Bremsstrahlung absorption was first examined by Mjolsness and Ruppel [7]. Their ordinary differential equation method is restricted to two ion species and does not include temperature equilibration. The MC code includes temperature equilibration and can handle an arbitrary number of species.

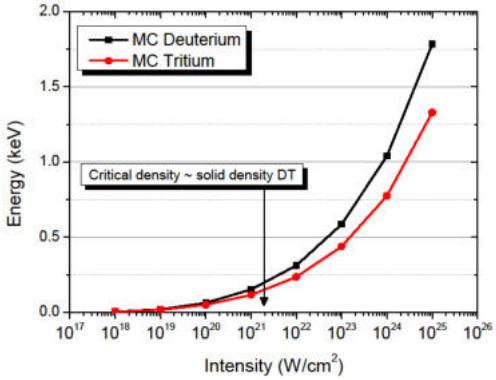

Fig. 3: DT, 500 fs pulse at critical density.

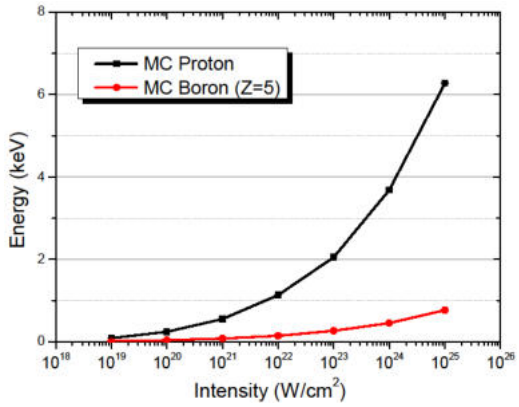

Fig. 4: pB, 300 fs pulse at critical density.

Fig. 3 shows the heating effect for two species of similar charge and mass. Using a high Z ion and a low Z ion pushes the low Z ion to much higher energies, as demonstrated in Fig. 4 with Boron. Fig. 5 also exhibits this effect, and shows how it applies to three ion species.

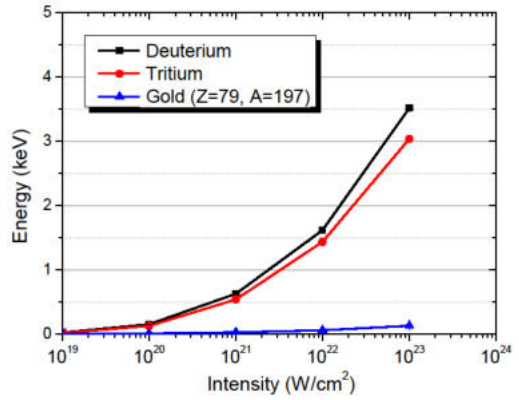

Fig. 5: AuDT, 30 fs pulse at critical density.

Conclusions

A full picture of the heating mechanism requires a model including the complex interplay of QED-plasma effects, but the MC simulations suggest that effective intensities of 10^{23} W/cm^2 applied for tens of fs can achieve energies in the keV via inverse Bremsstrahlung absorption with a suitable choice of ions. In future, more complex models and mathematical descriptions of ion-ion inverse Bremsstrahlung absorption will be sought, and a formal prescription for pulse shapes that maximise the heating rate provided.

References

1. S.-W. Bahk et al, *Optics Letters*, **29:24**, p. 2837, (2004)
2. C. P. Ridgers, C. S. Brady *et al.*, *Phys. Rev. Lett.*, **108**, 165006 (2012)
3. J. G. Kirk, A. R. Bell and I. Arka, *Plas. Phys. and Cont. Fus.*, **51**, 085008 (2009)
4. Y. Ping et al., *Phys. Rev. Lett.*, **100**, 085004 (2008)
5. T. Takizuka and H. Abe, *Journal of Comp. Phys.*, **25**, 205-219 (1977)
6. G. E. P. Box and M. E. Muller, *Annals of Math. Statistics*, **29:2**, 169-181 (1996)
7. E. M. Epperlein and M. G. Haines, *Phys. Fluids*, **29**(4), 1029 (1986)
8. R. C. Mjolsness and H. M. Ruppel, *Phys. Fluids*, **15**(9), 1620 (1972)

Achromatic Beam Diagnostic Telescopes for Astra Gemini

Contact *chris.hooker@stfc.ac.uk*

Chris Hooker

Central Laser Facility
STFC Rutherford Appleton Laboratory
Harwell Oxford Campus, Didcot, OX110QX

Introduction

During the design phase of Astra Gemini, it was decided to use commercially-available refracting telescopes with 150 mm aperture and 1200 mm focal length to focus the 150 mm diagnostic beams before and after the pulse compressors. Such instruments are readily available, surprisingly cheap and of reasonable optical quality: typical P-V wavefront errors measured on the four instruments bought for the Gemini project were ¼ wave in the visible. The drawback with them is that they are corrected for chromatic aberration in the visible spectrum, whereas the Astra beam lies in the near-infrared. During the early years of operation this was not a serious limitation, but over the last year or two the quality of the focal spot and the accuracy of the diagnostic used to measure it have assumed greater importance, so an improved optical system was needed. This article describes the systems that have now been installed on the compressed beam lines, and are due to be installed on the inputs to the compressors later this year.

Optical design

The main problem with the old telescopes was their chromatic error over the 30 – 35 nm bandwidth of Gemini. Based on a plot of the focal length variation with wavelength for a typical achromatic lens from a catalogue, the variation in focal position over the Gemini bandwidth was calculated to be around 0.45 mm at the focus of the telescope objective. The image is then magnified by a microscope objective with a working distance of 15 mm, which re-images the spot on a camera. The size of a monochromatic diffraction-limited spot formed by this optical system is about 300 microns; however, the variation in focal position due to wavelength causes the wavelengths away from the centre of the bandwidth to be focused well in front or behind the camera sensor, giving an out-of-focus disc more than a millimetre in diameter. The light distribution in the broadband image does not accurately represent the quality of the actual focal spot on the target, which is formed by an off-axis parabolic mirror.

Overcoming this problem requires either a 150 mm aperture achromatic lens that is properly corrected for the 770 to 830 nm spectral region, or an all-reflective optical system such as a Newtonian telescope. The reflecting system is the cheaper option, and as with the original refractors, many different instruments are available commercially at reasonable cost. However, they all suffer from the problem of a central obstruction in the light path, which affects the quality of the focal spot and prevents near-field imaging of the central portion of the beam. An alternative would be an off-axis parabolic mirror similar to those used for the final focusing optic, but such mirrors are far more expensive than conventional on-axis parabolas, and require more precise set-up and maintenance of their alignment.

The solution adopted was to buy a high-quality on-axis parabola from a telescope manufacturer, and use a full-aperture partially-reflecting beam splitter rather than a sub-aperture mirror to steer the focal cone to a place where it could be accessed easily. This design, illustrated in Figure 1, sends 90% of the light into an energy diagnostic, thus also protecting the imaging part of the diagnostic from the full energy of the diagnostic beam. The remainder is focused by the parabola, and after the converging cone is reflected from the beam splitter it forms unobstructed achromatic images of the near-field and far-field of the beam.

The parabolic mirrors were obtained from a UK telescope manufacturer, Orion Optics Ltd. They have a focal length of 1200 mm and a surface figure accuracy of ⅛ wave at 633 nm. To avoid any clipping of the beam or edge effects, a mirror of 200 mm diameter was chosen for the 150 mm beam. The mounts used to hold these optics are 8-inch manually-adjustable gimbal mounts made by Aerotech, which are thermally compensated for maximum stability, and have differential adjusters allowing very sensitive positioning. The 90% beam splitters were obtained from CVI Melles Griot, and were specified with a very low transmitted wavefront error to minimize distortion of the focal spot. The 90% coating is optimized over a 60 nm bandwidth at an incidence angle of ten degrees, and the other surface is antireflection coated. In the final setup, the AR coating faces the incoming beam: this is so the converging image cone is reflected from the 90% surface without having to pass twice through the substrate, which would introduce too much aberration. A second window sends a fraction of the converging cone to the far-field channel, while the remainder continues to the near-field camera.

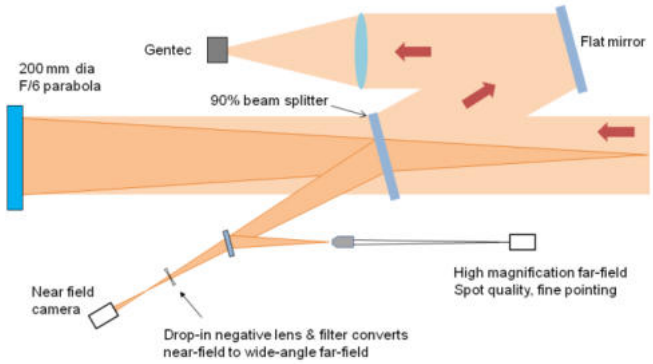

Figure 1. Layout of new design for Gemini beam monitoring telescopes.

Energy monitoring

The light rejected at the 90% beam splitter is used for energy monitoring, via an aluminium mirror and a lens which is actually the positive element of the original achromatic telescope lens. The converging beam is incident on a small-aperture energy-monitor (Gentec) to provide a measure of the compressor output energy. The Gentec readout is linked to the computer-controlled data acquisition system of Gemini so the reading can be recorded.

Set-up and alignment

The most important part of the alignment is ensuring the axis of the parabolic mirror is parallel to the incoming beam. In practice the mirror is working at F/8, and the region where the

focal spot is not detectably aberrated is about 10 mm in diameter. However, the 1% of the light that returns through the beam splitter to the prime focus of the mirror is bright enough to see with an IR viewer in transmission through a piece of paper when the paper is in the focal plane. With one of the alignment reference crosswires in the beam, the shadow of the crosswire can also be seen on the paper, and it is easy to adjust the parabola so the focal spot is centred on the cross. The error in this method is estimated at no more than half a millimetre, which is well within the region of tolerance.

Imaging section

The cone of light converging to the near-field camera is intercepted by a wedged window with antireflection coatings on both faces. The weak reflected beam from the front face is sent to the high magnification far-field channel, where the image is relayed at around 20x magnification onto the far-field camera. The high degree of attenuation provided by the AR coating is necessary to avoid nonlinear effects at the focus in front of the objective when the laser is fired at full energy. It also makes the beam so weak that the setup is difficult to align, as the CW beam cannot be seen with a viewer except in total darkness. In practice the window was replaced by a mirror for initial alignment, then the window was reinstalled for the final adjustments. The final version of this channel will use a window with one uncoated face, and the stronger beam reflected from that face will be sent to a photodiode to provide a whole-beam prepulse monitor.

The beam diagnostic suite is required to produce near-field and far-field images of the beam under various conditions. In particular there is a requirement for focal spot imaging in all the power modes of the laser, i.e. CW, low-, medium- and high-power and full-energy shots. To achieve this, computer-controlled filter wheels with appropriate neutral density filters are positioned in front of the cameras at places away from a focus. The filter wheel position is set by the camera control software according to the energy mode of the laser.

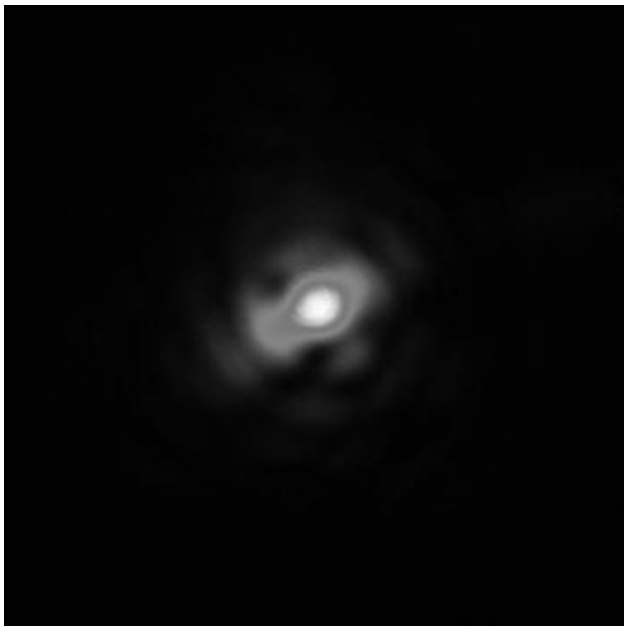

Figure 2. Example far-field image from the old telescope system.

The improvement in image quality can be seen in Figures 2 & 3, which are respectively from November 2011 when the old telescopes were still in use, and February 2012, after the new telescope was installed in the north beam. Both images are to the same scale, and have been enhanced to show some of the fainter light distributed around the central spot. In the later image the size of the central spot is smaller and the amount of light around it is significantly reduced, which is as expected given the absence of chromatic aberration in the new telescope design. Both images show a small amount of astigmatism, but this is present on the beam and was not introduced by the imaging systems.

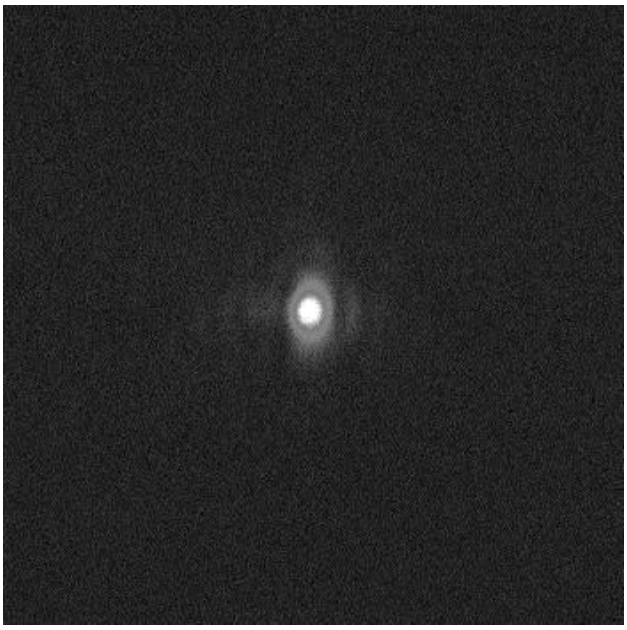

Figure 3. Example far-field image from the new telescope system.

Wide-angle far-field camera

The field of view of the high-magnification far-field telescopes is so small that locating the image is a significant problem, especially as the image beam is very weak after being heavily attenuated. If the alignment changes slightly for any reason, the far-field image can disappear, but the near-field image has not moved visibly and gives no useful information about the size or direction of the displacement. To overcome this problem, and significantly improve the ease of operations, the near-field imaging channel can be converted into a wide-angle far-field channel by inserting a negative lens in the position shown in Figure 1. This moves the position of the focus back to the plane of the camera sensor, and the resulting field of view is about 30 times larger than the high-magnification far-field channel. Once the high-magnification channel had been aligned correctly, the drop-in lens was positioned to centre the spot on the near-field camera so the two channels were co-aligned. The negative lens and a neutral filter (ND 3.0) are mounted in a common holder on a kinematic baseplate, so the lens can be inserted or removed as required without any need to change the filtration in front of the camera.

The benefits of this capability are significant. Optimizing the alignment of the compressors frequently requires equal and opposite movements to be made on the two gratings, with the far-field imaging system being used as a beam pointing reference to ensure the gratings remain in the same relative position. To minimize the risk of losing the alignment, the normal procedure for this required the spot to remain visible at all times, which meant that only very small movements could be made. The availability of the wide-field camera allows much larger movements to be made with the confidence that the beam pointing can be easily restored, greatly speeding up the process.

Recent improvements in contrast on Astra Gemini

Contact *chris.hooker@stfc.ac.uk*

Chris Hooker, Oleg Chekhlov, Steve Hawkes, Bryn Parry, Rajeev Pattathil & Yunxin Tang

Central Laser Facility
Rutherford Appleton Laboratory, Harwell Oxford campus, OX11 0QX

Introduction

The contrast of the pulses delivered to target by the Astra Gemini laser has been the subject of a significant campaign of work over the past two years. Poor contrast can result from background ASE levels, ns-scale prepulses or copies of the main pulse arriving in the 200 ps before the principal peak, but whatever the source, the effect is to degrade the interaction with the target by generating a pre-plasma or affecting the properties of the target surface. In ultra-thin foil experiments the presence of quite low levels of pre-pulse is sufficient to destroy the target entirely, preventing any meaningful science from being done. Over the past two years a systematic campaign of identifying and eliminating the source of prepulses has made significant improvements in the contrast of the pulses from Gemini. The majority of these changes involved replacing broadband AR coatings with narrow-band types on windows, lenses and polarizers, to minimize post-pulses from these components. This in turn minimizes the conversion of post-pulses to pre-pulses that occurs by the well-known nonlinear phase coupling mechanism[1]. During the campaign other changes were identified that required special optics to be purchased, and over the past year several of these have been completed.

Recent changes in the Astra laser

In the past year we have rebuilt amplifiers 1 & 2 to a new design that allows the use of wedged Ti:sapphire crystals. This work is described elsewhere in this report[2]. The effect of these changes has been to eliminate several of the more troublesome discrete prepulses, including the Ti:sapphire anomaly pulses that are generated in the crystals by a mechanism that is not understood.

Another group of prepulses at -62 to -63 ps originated from double reflections in the windows of the vacuum spatial filters in amplifier 3. Eliminating these required the introduction of wedged windows, which is potentially problematic in a broadband laser because of the dispersion that the wedges introduce. However, wedged windows can be used provided they are in matched pairs, such that the wedge of the input window is opposed to that of the output so there is no net angular dispersion. In practice this means that the two wedges are orientated in the same direction, because the beam is inverted as it passes through the VSF. To ensure equality of the angles, a single large wedged optic was made, and a dozen 2-inch diameter windows cut from it. The resulting components are not all the same thickness, but this in practice has a negligible effect on the pulse duration, as the windows are ¼ inch thick and have wedge angles of only 2 arc minutes. The amount of spatial chirp that one pair introduces is completely negligible, and in any case the optics around the laser are such that the spatial chirp of one pair of windows cancels out that of the other. The result can be seen in the partial Sequoia scan presented in Figure 1: the red trace was recorded before and the blue trace after the windows were replaced, and the -62 ps prepulse has disappeared. There are eight other ¼ inch windows in the laser: in the beam pipe between Astra and Gemini, and in the VSFs in the Gemini amplifiers. These are believed to be the source of the weaker prepulses between -63 and -65 ps in the trace.

Prepulses from beam splitters

There are two beam splitters in the Astra laser chain. One is placed after amplifier 2 to provide a 10% split for the probe beam that is used in Target Area 2, and the other is the 50% splitter that generates the two Gemini beams from the single Astra input beam in the Gemini laser area. The strength of the double reflection from a window is the product of the reflectivities of the two surfaces, so a beam splitter inevitably produces a larger post-pulse than a window, as only one surface can have an anti-reflection coating. The TA2 probe beam splitter has been shown to generate the fairly strong (10^{-6}) prepulse at -30 ps, and the 50% splitter is the source of the -90 ps prepulse that appears at a few times 10^{-6}. To eliminate these prepulses requires the use of wedged beam splitters, together with matched compensating wedges with identical angles that have high-quality AR coatings on both sides. These optics have been obtained in the past year, and the first pair, replacing the TA2 probe splitter, have been installed after the second amplifier of Astra. As with the VSF windows, these components were cut from single wedged optics to ensure equality of the wedge angles. At the time of writing we have not verified by means of a Sequoia scan that the -30 ps prepulse has been eliminated, but the double reflections within the wedges will definitely be rejected at the spatial filters in amplifier 3, so there will be no opportunity for the pre-pulses to be generated.

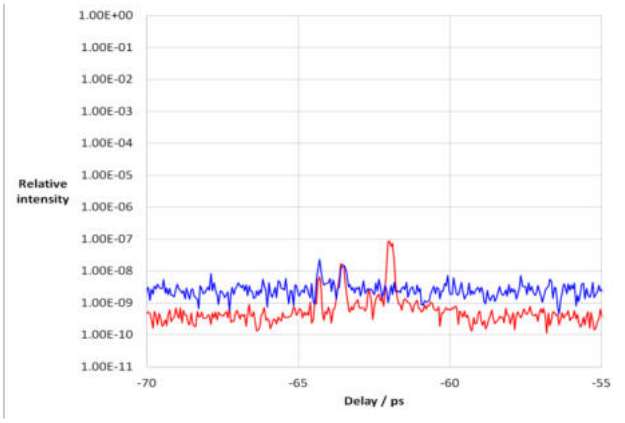

Figure 1. The effect of replacing plane-parallel windows with wedged windows in the amplifier 3 VSFs. Red trace: before replacement; blue trace: after replacement.

References

1. N.V. Didenko, A.V. Konyashchenko, A.P. Lutsenko, S.Yu. Tenyakov, Optics Express **16** (No 5), 3178-3190, March 2008

2. B. Parry, Y. Tang, C. J. Hooker, S. J. Hawkes, CLF Annual Report 2012, pp 61

Development of an Adaptive Optic System for Use in the Astra Gemini Target Area

Contact *dan.symes@stfc.ac.uk*

J D Alston, P S Foster, M Galimberti, C J Hooker, R P Pattathil, K Poder, D R Symes

Central Laser Facility, STFC Rutherford Appleton Laboratory, HSIC, Didcot, Oxon OX11 0QX

S Bonora

Department of Information Engineering, University of Padova, Italy

Introduction

Unaberrated beams are key to Astra Gemini achieving high intensity laser focal spots. One method that has been explored is the use of adaptive optics (AO) in the target area to flatten the wavefront. The AO system involves the use of a 200mm diameter deformable mirror and a wavefront sensor to correct the phase of the beam. There are two main scenarios in which the system was intended for use if it could be shown to be effective. The first was the reduction of aberration in the 150mm beam going onto an f/2 off-axis parabola, in order to improve the energy contained within the focal spot. F/2 parabolas are the focusing optics used for the majority of the high intensity, solid target experiments conducted in Astra Gemini at the moment. The other use of AO is with a novel method of fielding a shorter focal length f/0.87 on-axis parabola in place of the f/2. This parabola should result in a smaller focal spot size and therefore increased intensity if the beam quality can be maintained. Difficulties, which are discussed in detail later, in the arrangement of optics required to use such a short focal length on axis parabola mean that an AO system is required for good beam quality to be realised. This report focuses on the latter use of AO though work is on-going on both applications.

Apparatus

The deformable mirror used for testing was a made from a thin substrate coated with gold on one side and a piezoelectric actuator pattern on the other. It has 61 actuators and the pattern spanned approximately 200mm. The wavefront sensor used was Phasic SID4 device; it uses a method called lateral shearing interferometry to measure the phase of the beam. This is an advanced variant of the Shack–Hartmann wavefront sensor. It gives wavefront information with a resolution of 160 x 120, and is wavelength independent.

Software

The interference pattern measured by the SID4 wavefront camera is processed by the accompanying software written by Phasics in order to extract the wavefront from it. A software development kit (SDK) for use in LabVIEW is provided. Using this SDK, software was written in LabVIEW to manipulate the phase information from the camera, and to combine it with the movement of the deformable mirror's actuators to produce an AO system. The code works in a standard AO way; first it collects the influence function by moving each actuator individually and recording the resulting phase change, then it uses this information combined with a wavefront measurement of the beam to calculate the voltages required to be applied to the actuators in order to get a flat wavefront. The software filters out any tilt or defocus aberrations from the phase maps before computing the correction, which means that the AO system will not try to correct for any tilt or defocus in the beam. The wavefront resulting from the correction is then analysed and the process iterated to achieve a good correction.

Circular Beam Adaptive Optics

The arrangement and apparatus used for testing the adaptive optic system in this report was based around that shown in Figure 1. It consisted of a collimated laser with a super-Gaussian intensity profile and good phase quality with low levels of aberration (less than 0.05 waves of any single aberration).

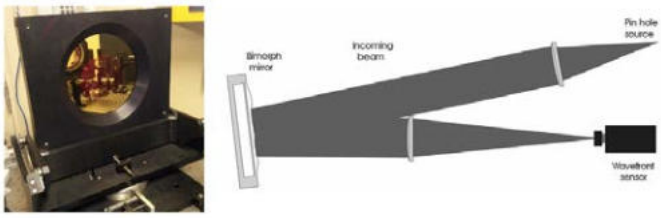

Fig. 1. Left: a picture of the deformable used in this report. Right: the approximate layout used for all of the testing, showing the collimated beam being reflected by the DM, being focused down, and then collected by the wavefront sensor.

Quality of circular beam correction

When an optic is introduced into a beamline the wavefront will always be aberrated to some extent. For the very high quality mirrors used commonly in the Astra Gemini target area the aberrations are generally undetectable, but for a deformable mirror they can be very noticeable. This is mainly due to the mirror substrate being much thinner and inherently more flexible, and the processes it experiences in production, such as the attaching of the piezoelectric crystal to the back of it. Therefore when the mirror is at rest it is likely to make the aberrations in the beam worse. If the beam already has quite a flat wavefront then it is possible that when the adaptive optics system is added it will not be able to be made as flat as the original wavefront, so no improvement could be made. It is therefore of interest to know how flat the DM can be made.

In order to test the fineness of the correction, a beam with the best possible phase quality was created. In this case the issue is not how well the mirror corrects the beam's phase, but how well it can correct for its own deformities. For this test the phase of the beam was diagnosed by placing the SID4 wavefront sensor in the near-field after the focus of a 3.5m focal length lens.

Table 1 and Figure 2 show the improvement in wavefront when the AO system was run. Also included in the table are the measurements of the raw expanded beam used for testing, without the deformable mirror in the beam line. It can be seen that the AO was able to correct the wavefront back to close to the quality it was originally, but would not be able to improve the focal spot. The level of aberrations introduced by adding the deformable mirror in its relaxed position is very noticeable, but the mirror is easily able to move enough to correct for the magnitude of the deformities in its relaxed profile.

	Astig 0^0	Astig 45^0	Coma X	Coma Y	Spherical	Strehl
Raw	-0.05	0.00	0.00	0.03	0.06	0.92
Before	0.23	0.10	0.09	-0.15	-0.09	0.53
After	-0.06	0.02	0.06	-0.06	-0.00	0.89

Table 1. The aberrations and Strehl ratio of a circular beam; with no deformable in the beam in the row labeled raw, with the DM at rest in the before row, and the DM in its best corrective position in the after row. Aberrations are given in waves.

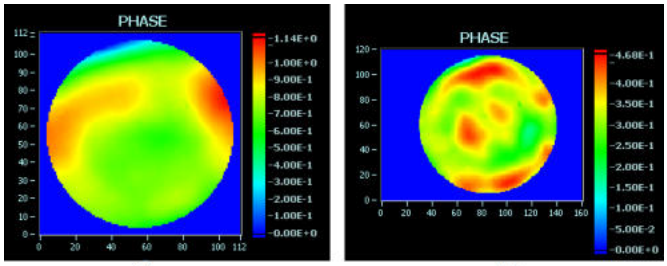

Fig. 2. (a): The phase of the beam with adaptive optics installed but at rest. (b): The phase after correction, note the difference in scale.

Use with the f/0.87 parabola

In order to use the f/0.87 on-axis parabola an arrangement like the one shown in Figure 3was proposed. This arrangement allows the target to be positioned in the focus of the laser but outside of the unfocused incoming beam. The use of a thin mirror to direct the beam on the parabola maximises the space behind the mirror that can be used for diagnostics for the interaction, however, this thin mirror is the main source of deformation of the wavefront. The thin mirror is only 4 mm thick compared with a thickness of approximately 24 mm for the other mirrors used in the beam line. The interferogram of the thin mirror shown in Figure 4 shows the way it distorts the wavefront of the beam.

The solution to the problem of the deformed thin mirror is to use the adaptive optic system to make the deformable mirror's surface into the opposite shape to the thin mirror, while also correcting for any other aberrations that may be present in the beam. The issue with using the existing AO system was that it could only deal with circular beams, because the standard software was not able to process annular beams.

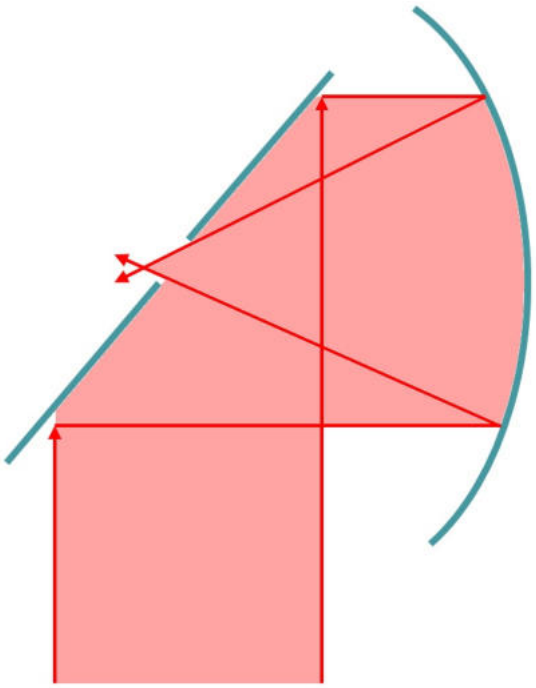

Fig. 3. Schematic of how the beam is directed onto the f/0.87 parabola and then focused through the central hole in the thin mirror.

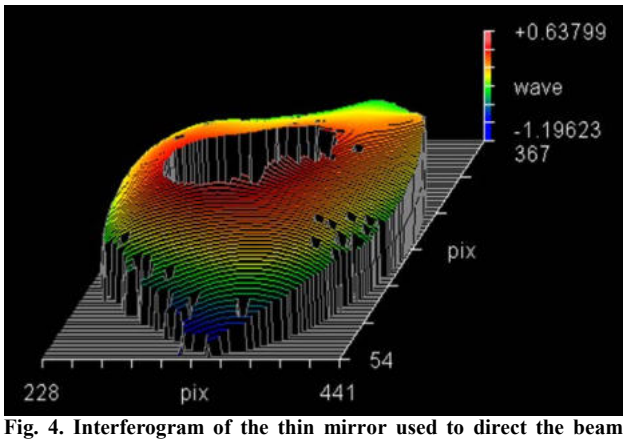

Fig. 4. Interferogram of the thin mirror used to direct the beam onto the parabola.

Annular beam correction

Using an on-axis parabola inevitably results in having a hole in the beam. In order for adaptive optics software to function properly it needs to have phase information for the entire masked region. When the thin mirror arrangement is used it results in a hole in near the middle of the beam creating an annular beam shape. A more complicated set of Zernike equations need to be used to correctly model the aberration of the beam in this case, the circular beam is a special case of the annular Zernike polynomials where the central hole's size is set to zero [1].

In order for the AO code to be able to acquire and process annular phase maps an updated version of the Phasics software was required. The updated version had many changes to the way sections of the code functioned, which in turn meant that many modifications were necessary to the way they were used and how they communicated with each other. The use of the annular masking and Zernike beam filtering were largely untested functions of the software, so work had to be done in collaboration with Phasics in order to get it functioning properly.

Quality of correction

This testing used almost the same conditions as for the quality of circular beam correction described earlier. The only notable difference was the annular software masks used. The beam with the adaptive optic system installed had a phase as shown in Figure 5. Both circular and annular masks were applied to the beam for comparison. The two phase maps seemed fairly consistent with each other, and their low order Zernike analyses are quite similar. Table 2 shows how the measured aberrations compare.

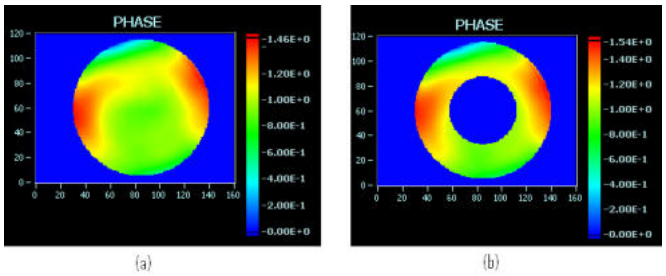

Fig. 5. (a) Shows the phase of the beam with the DM at rest. (b) Is the same beam but with an annular mask applied.

	Astig 0^0	Astig 45^0	Coma X	Coma Y	Spher.	Strehl
Circular	0.36	0.20	0.09	-0.14	-0.11	0.38
Annular	0.41	0.18	0.09	-0.16	-0.11	0.28

Table 2. Comparison of the Zernike coefficients of the aberration measured in the beam when using a circular and an annular mask.

Some very good influence functions were gathered, which when analyzed looked very smooth. Figure 6 shows the influence function of actuator 57, one near the edge of the mirror. The picture shows clearly the effect of the movement is not just localised to the region around the actuator, but actually extends right across the mirror, giving a raised region on the opposite side from the actuator. Despite the high quality influence functions the correction achieved was not as good as expected. The results of the correction can be seen in Figure 7. The beam starts off with a Strehl ratio of 0.92, but when the extra optics are introduced this falls to 0.38. This was expected as extra mirrors, and the deformable mirror were added. After running the AO software the Strehl ratio improved to 0.75 in the best cases. When a series of correction loops were run, starting from the relaxed position, they would not converge to a stable set of voltages. After achieving a reasonable correction with a few iterations, if further loops were executed the wavefronts often became more deformed. The Strehl ratio mentioned above was taken after only a few loops of the software, at the point where the wavefront quality peaked. When a series of corrections was run, starting from the relaxed position, quite different results were achieved, in terms of the amount of astigmatism and coma. However, the spherical aberration always remained consistently negative, and tended to increase in magnitude as more iterations of correction were done. Sometimes the Strehl ratio would only peak at around 0.6 and other times it would exceed 0.7.

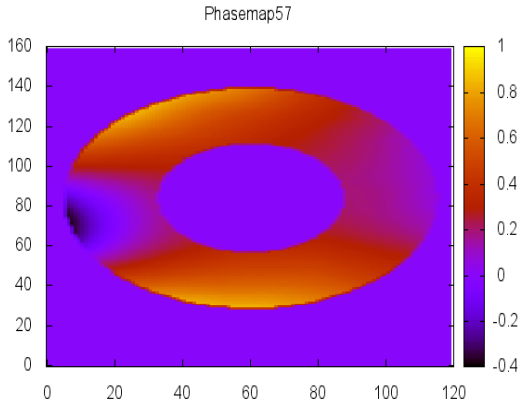

Fig. 6. This picture shows the influence function for an actuator near the edge of the mirror. The colours represent the relative heights of the wavefront, the scale is in units of waves.

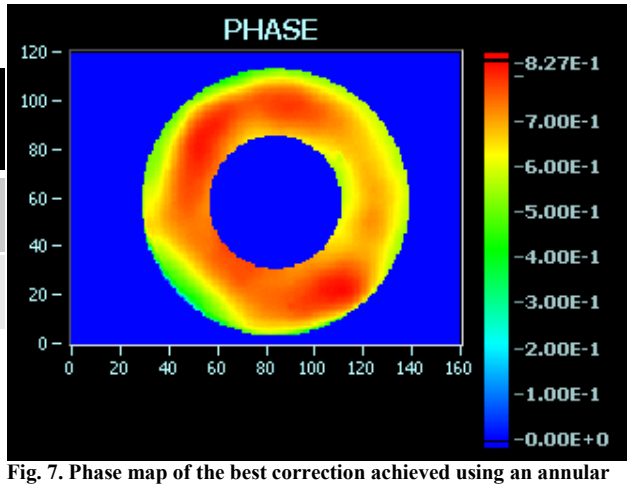

Fig. 7. Phase map of the best correction achieved using an annular mask. The scale is in waves.

	Astig 0^0	Astig 45^0	Coma X	Coma Y	Spher.	Strehl
Before	0.41	0.18	0.08	-0.15	-0.12	0.28
After	0.03	-0.05	0.08	-0.01	-0.17	0.75

Table 3: Comparison of the Zernike coefficients and Strehl ratio of; the beam with the AO system installed but at its rest position, and the beam after correction has been made.

Discussion

Comparison of the phases measured with circular and annular masks shows only minor differences. The main difference was the calculated Strehl ratios: the circular mask gave 0.38 but the annular one only 0.28. The phase map shows most of the phase error in the outer parts of the beam, so this may explain why the circular beam scores higher, as it has a flatter section in the middle. There is some possible error in these phase maps due to the way they are processed within the Phasics software, because it was set to filter out the defocus from the beam. It is likely that defocus cannot be so precisely filtered from an annular beam since it is missing the central region. The software is more likely to confuse a combination of other higher order

aberrations for defocus in the annular case. This does not appear to be a major problem in the circular versus annular masked phase measurements compared here however.

The exact geometry of the thin mirror-parabola arrangement means that the hole in the thin mirror is not actually central on the beam. This is because of the way the plane of the mirror cuts through the cone of light focused by the parabola at an angle. By making the mirror's hole match this angular cone slice profile the circle is shifted off-centre on the incoming beam. AO corrective software that is based upon the Zernike polynomials is limited to symmetrical annular mask shapes: they cannot have an off-centre hole because the polynomials would not fit. This gives two options for fitting the mask shape to the beam, either make the hole larger and centre it on the outer beam shape, or centre it on the hole and reduce the outer circle's radius. Both result in parts of the beam being excluded from correction, and in fact the areas of beam not inside the mask will be deformed, since the actuators corresponding to those regions will be moved during the correction in order to achieve the best correction on other parts of the beam where they have some influence.

Thin mirror correction

There was uncertainty whether the deformable mirror would be able to produce correction of the magnitude required to compensate the errors of the thin mirror. The correcting power of the deformable mirror is not absolute. Each actuator has the ability to deform the surface, but when combining the movements of multiple actuators the limits to which the surface can be moved is not simple to estimate. The most basic limitation is the maximum gradient of the wavefront that can be corrected. If the thin mirror had a small but steep bump in it, it is possible that although the magnitude of the wavefront error would not be too large to correct, the surface of the mirror is not flexible enough to be deformed to match it. It can be seen from the influence functions that a single actuator has the ability to move approximately 1.5 waves, which is roughly 1 micron. When working together to correct a smooth, low order aberration such as astigmatism, peak to valley deformations of greater than 7 waves can be achieved. Looking at the interferogram in Figure 4 the deformation appears to be largely a curvature over the whole surface. This corresponds to defocus in the beam. The AO system was set to not correct for the defocus aberration since it doesn't deform the focal spot, (it only moves its position), so the DM must only correct the remaining aberrations.

Finally, it should be stated that the testing of the correction for the thin mirror was done using a different beam from that used in previous tests. This beam was not such high quality: the intensity profile was less even, the aberration levels were higher, and it was not as well protected against air turbulence.

Results

There were many difficulties found in trying to correct the beam. One of the first issues was producing a suitable beam after focus to measure the wavefront at. This problem was due to a combination of the thin mirror being deformed by the way it was mounted and, to a lesser extent, the actual deformities of the surface of the mirror when under no pressure. In initial testing the point at which the beam was being measured was a pseudo-far-field, with the effects of aberrations extending further than normal from the focal spot location due to the magnitude of the wavefront deformities. The problem was exacerbated when corrections started to be run using the adaptive optics, adding large deformations of the DM as well. This problem was solved by adding an extra lens to achieve the correct imaging.

With the imaging plane adjusted the beam fitted well onto an annular mask. The hole in the middle of the beam was bigger, and more elliptical, than it would be when used in the experimental f/0.87 layout because the beam was not reflected off the mirror at the full 45^0. Fitting a circular shape onto the ellipse in the middle meant that the annular ring mask was thinner than would be used in the correct layout.

When the AO system was run, after only a few loops the voltage being applied to some of the actuators would reach the maximum 60 volts. It could be seen that after this point it was uncommon for further improvement of the wavefront to be made. After approximately 10 loops the majority of actuators would be at the maximum 60 volts and the aberrations of the wavefront would be much worse than after only a few iterations of correction.

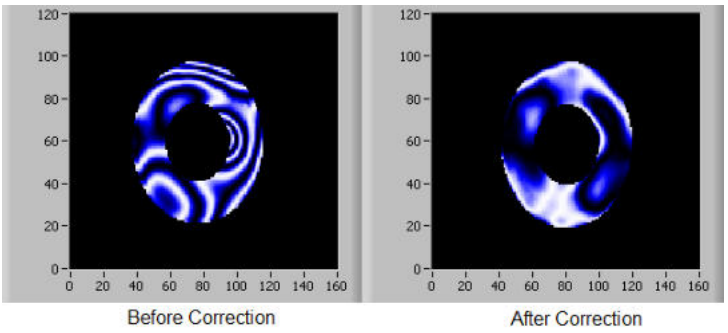

Fig. 8. The phase maps before and after correction when the thin mirror was in the beam. There is a π phase difference between regions of black separated by white.

	Astig 0^0	Astig 45^0	Coma X	Coma Y	Spher.	Strehl
Before	0.36	-0.51	0.32	-0.39	-0.10	0.11
After	0.20	-0.12	0.02	-0.08	-0.15	0.44

Table 4. The aberrations and Strehl ratio of the beam reflected of the thin mirror before and after AO correction was done.

Discussion

There was large improvement in wavefront flatness, however the flatness achieved was much less than in the previous test to find the limit of correction fineness. This was due to the beam being too aberrated to correct; the actuators on the mirror simply could not deform the surface sufficiently. The quality of correction might also have been slightly affected by the less precise influence functions, due to greater air turbulence.

The phase before correction looks quite different from the interferogram of the thin mirror shown in Figure 3. This was expected since the defocus had been removed from the measured phase, but the remaining aberrations are also larger than predicted. These extra aberrations are possibly from a lens in the system that was faulty. It was found that rotating one of the lenses caused a change in the aberrations present. No further progress can be made until the aberrations in the beam are reduced to levels correctable by the deformable mirror. A flatter thin mirror would be needed for this to be achieved. A possible reason why this mirror was so deformed is that one side has been silver coated while the other has not. The coating process can introduce stress, so coating both sides of the mirror should balance out the stresses. However the effectiveness of this may be limited because it was the higher order aberrations that could not be corrected rather than the overall curvature of the mirror.

It is possible that these aberrations were an unlucky result of various aberrations already present in the beam and DM that when combined with those of the thin mirror were too large. Therefore it is important in the future to measure what the beam is like before adding the thin mirror so that the constructive addition of aberrations can be avoided if possible.

Conclusions

The pre-existing adaptive optics system has been tested and corrections resulting in a circular beam with a 0.89 Strehl ratio have been achieved. The AO code was modified to work with annular beams, in order to be used in conjunction with a short focal length on-axis parabola with the aim of reducing the focal spot size, thus increasing intensity. Correction of annular beams was achieved but not ideal: the algorithms do not seem capable of removing spherical aberration from the wavefront. Despite this problem a maximum Strehl ratio of 0.75 has been achieved for annular beam correction, meaning a 20% loss in focal spot intensity when compared with the best circular beams achieved in testing.

The AO system was used to try and correct for the thin mirror which would be used to direct the beam onto an f/0.87 on-axis parabola. Some improvement was made, but the magnitude of the deformation of the wavefront was too large for the deformable mirror to correct fully.

There are many flaws with the principle of moving from the use of an f/2 off-axis parabola to an f/0.87 on-axis parabola that reduce the capacity for focal spot intensity improvement. They include the change in far-field beam intensity profile to one where there is less energy in the central spot, the off-centred mask that limits the area of the beam that can corrected, and the greater difficulty in correcting an annular beam. The resulting loss in intensity due to these problems is difficult to predict, only experimental results with a flatter thin mirror and the f/0.87 parabola would confirm whether the intensity can be increased. Some of these problems could be overcome by implementing the adaptive optics in a different way. For example if the phase of the beam were measured after the DM but before being reflected off the thin mirror it would still be circular. This could be done by measuring the wavefront of the beam transmitted through a dielectric mirror at a suitable point in the system. The deformation to the wavefront due to the thin mirror must still be taken into account, and this could be achieved by measuring the thin mirror's shape with an interferometer and adding that error to the measured wavefront before applying the correction. Another possible route to correcting the annular beam more precisely is to use an AO system based on maximising focal spot intensity rather than directly maximising wavefront flatness. Both of these alternative methods have their own problems, but unless the spherical aberration problem with the current AO software can be fixed the quality of the wavefront will always be less than ideal, reducing the focal spot intensity by 20%.

Acknowledgements

Stefano Bonora should be acknowledged for the large amount of work he did writing the adaptive optic code, which was edited by the author to work with annular beams.

References

1. X. Hou, F. Wu, L. Yang, and Q. Chen, 2006, `Comparison of annular wavefront interpretation with Zernike circle polynomials and annular polynomials,' Appl. Opt. 45, 8893-8901.A reference

Replacement of Astra Amplifiers One and Two for Enhanced Laser Contrast

Contact *bryn.parry@stfc.ac.uk*

B. Parry, Y. Tang, C. J. Hooker, S. J. Hawkes

Central Laser Facility, STFC Rutherford Appleton Laboratory
Harwell Campus, Oxfordshire, OX11 0QX, UK

Introduction

In high intensity laser plasma experiments, one key parameter is the contrast ratio between the main laser pulse, and the background or discrete pre-pulses. This temporal contrast must be sufficiently good to avoid forming a pre-plasma on the target before the ultra-short compressed pulse arrives, otherwise the interaction physics will be significantly altered.

The Ti:Sapphire amplifiers in the Astra laser are responsible for introducing pre-pulses on ns down to few ps timescales, at levels up to ~10^{-6} of the main pulse. Following the replacement of the third amplifier in 2009[1], several of the pre-pulses due to components in this amplifier were reduced. It was thought that the key change was the introduction of spatial filtering between passes of the crystal. To extend these benefits to the remainder of the laser chain, as well as addressing general issues of performance and stability, it was decided to upgrade the first two multi-pass amplifiers in the same style.

New amplifier design

Apart from the redesigned third amplifier, the other Astra amplifiers have remained largely unchanged since their construction at the end of the 1990s. The most significant upgrade has been the addition of automatic alignment[2].

In order to integrate the new amplifiers into the existing system, the optical layout was designed in 3D CAD software, allowing analysis of mechanical and optical constraints to the physical layout. Figure 1 shows amplifier 1 within the existing system, including the stretcher enclosure.

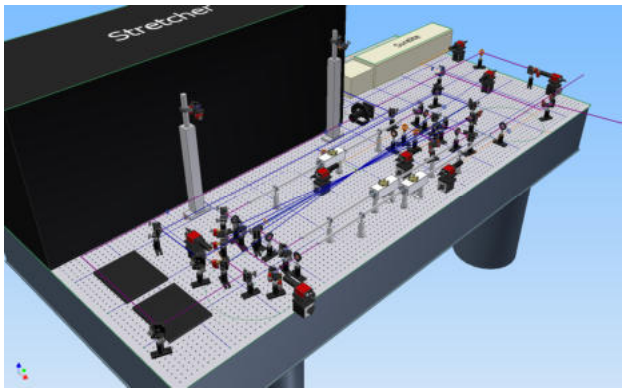

Figure 1: CAD model of new amplifier 1 design

Optical modeling was carried out using a one-dimensional code developed in house. This was used to simulate the performance of the new amplifier 1 in a 4-pass configuration. In the code, it is assumed that both the pump and seed pulses are spatially and temporally uniform with a top-hat beam profile throughout the amplifier, and the spatial overlap between the pump and seed in the laser medium is ~80%. The total cavity coupling of the amplifier is estimated to be around ~90% by taking into account surface reflections of optical components and loss in the laser medium. A 7 mm long Ti:S crystal with absorption coefficient of $\alpha \approx 3.3$ is used, giving an absorption of ~90% per pass. The pump beam diameter is defined at 2.5 mm. In the Astra laser system, the energy of the seed pulse into amplifier 1 is about 90 µJ. Under those conditions, the simulated performance of the new amplifier 1 is shown in figure 2. below. As can be seen, at the normal pump energy of 90 mJ, the new amplifier 1 is capable of delivering output energy of 4 mJ.

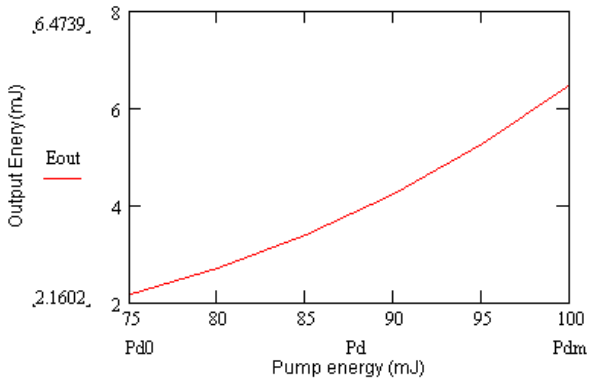

Figure 2: Gain modeling for amplifier one

Contrast design considerations

Pre-pulses on ns timescales are created by scattering within the multi-pass amplifier, such that the light enters subsequent passes before the main pulse. It is believed that the major source of these is from the Ti:S crystal in the forward going direction. Assuming that the amount of scattered light decreases at larger angles, the best way to minimise scatter pre-pulses is to increase the angular separation of beams traveling through the crystal in the same direction. This was done in the new amplifiers by having the closely angularly spaced beams going in opposite directions through the crystal, as shown in figure 3.

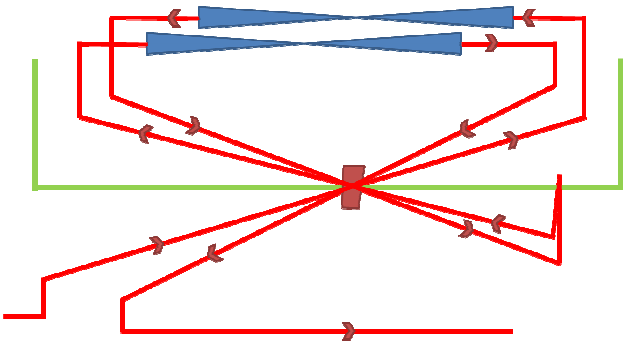

Figure 3: Schematic of amplifier 2 layout

The primary source of pre-pulses on ps timescales is slightly more complex, resulting from the initial generation of post-pulses by double reflections in optics. The reflection from two AR coated surfaces causes a weak post-pulse replica of the main pulse, for broadband AR coatings this can be as much as 0.25%. Due to the fact that this is a CPA system, the stretched pulse and post-pulse are substantially overlapped. When they pass through components there will be a nonlinear phase shift which leads to modulation in the spectrum, generating sideband frequencies. When the pulse is recompressed, the outcome is the formation of a pre-pulse at a time equal to the delay of the post-pulse[3]. The magnitude of the pre-pulse is proportional to

the post-pulse and the square of the B-integral through the chain after the point it is generated. There is little scope for significant improvement in the B-integral on Astra-Gemini, so the size of the post-pulse must be minimized in order to enhance contrast.

Any optic with two sufficiently parallel surfaces in the beam path can generate post-pulses which will propagate to the end of the system. Practically, this means windows, beam splitters, and the Ti:S crystal. Modern narrow band anti-reflection coatings can achieve reflectivities less than 0.1% over the bandwidth of Astra. However in the case of the Ti:S crystal, it must be considered that even a weak reflection will experience gain through the active medium, so can be many times greater than would be expected. Even better AR performance can be obtained by using p-polarised light with surfaces at Brewster's angle, though this becomes less practical for larger components, or expensive materials such as Ti:S.

The solution chosen for the Ti:S was the introduction of a wedged crystal to replace the previous plane parallel one. Combined with spatial filtering, this blocks the post-pulse from progressing through the amplifier chain. The design of the amplifiers needed to avoid introducing angular dispersion and spatial chirp from passing through the wedged crystal. This was done by having an even number of passes (four), with the beam orientated so that successive passes were in opposite orientations hence cancelling out the dispersion. The new spatial filters were designed with windows at Brewster's angle. Large f-number (>*f*/180) lenses were used to minimise the aberration introduced by the angled glass in the converging beam. The beam is fully image relayed by the VSF telescopes back onto the crystal position, improving the stability of the system. The arm lengths between passes are sufficiently long to avoid the ~5 ns chirped pulse overlapping with itself in the crystal, a deficiency of the old amplifier 1 design.

Amplifier Performance

The new amplifier 2 was commissioned in June 2011, amplifier 1 was replaced in the next maintenance period in October. The completed amplifier 2 is shown in figure 4.

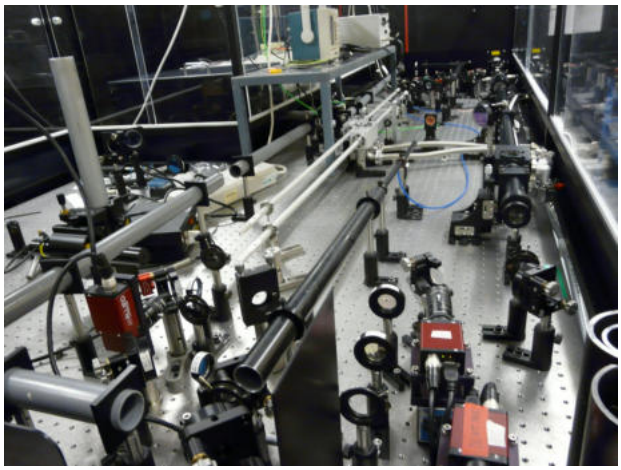

Figure 4: The completed new amplifier 2

The pump lasers for both amplifiers remain the same as previously used; a Continuum Surelite delivering 90 mJ for amplifier 1, and a Spectra Physics Quanta Ray providing 600 mJ for amplifier 2. The pump imaging to the crystal was modified slightly, and the beam path enclosed with pipes where possible for safety considerations, but the pumping was otherwise unchanged.

The output from amplifier 1 reached over 3 mJ in commissioning, but reduced input levels due to higher than expected losses in the stretcher have meant the output is typically 2 to 2.5 mJ. Amplifier 2 produces ~150 mJ from the final pass, which after expansion through a VSF and circular apodisation by a serrated aperture is reduced to ~130 mJ. The gain of the fourth pass is somewhat lower, indicating that the amplifier is working slightly in saturation. This mode of operation improves the output energy stability.

In both amplifiers, the automatic alignment system to compensate slowly varying (e.g. thermal) drift in alignment was reinstated.

Contrast Improvement

Contrast was measured at the system output after compression. The ns contrast was captured on fast photodiodes attenuated with calibrated neutral density filters. The ps contrast was measured using a scanning third-order cross-correlator (Sequoia, Amplitude Technologies). To allow scans to be completed in reasonable time, it was measured with the 10 Hz output of the Astra laser (amplifiers 1, 2 & 3). We have previously verified that contrast is not significantly different when also running the final Gemini amplifiers[4].

The improvement in contrast following the construction of the new amplifiers is shown in figure 5.

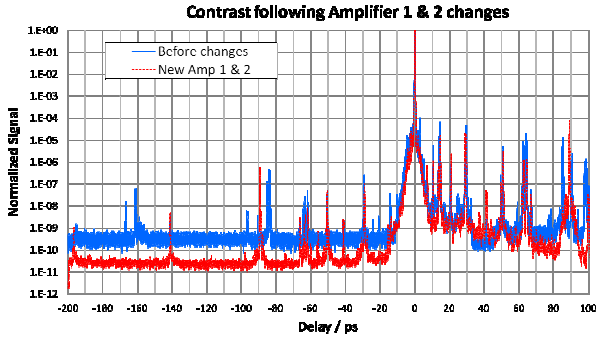

Figure 5: Contrast improvement on the ps timescale

The reduction in the ASE baseline can be attributed partly to the improved spatial filtering, but is very close to the noise floor of the instrument, so is also affected by internal alignment of the Sequoia. The most noticeable improvement is due to the wedged Ti:S crystals. The 7 mm amp 1, and 14 mm amp 2 crystals were responsible for pre pulses at ~167 and 83 ps. In addition to the replica pulse expected from a double reflection, the amp 2 Ti:S also produced a longer 'feature' over a few ps, around 162 ps, the origin of which is unknown. All these features are eliminated in the later scan, with no additional pre-pulses around 118 ps which could be expected from the 10 mm thickness of the wedged crystals.

The pre-pulse at ~90 ps is due to separate changes made to the 50/50 beamsplitter at the input of Gemini. This is scheduled to be replaced with a wedged splitter and matched dispersion compensating AR coated glass wedge.

Conclusions

We have successfully replaced the first two multi-pass amplifiers in the Astra laser chain with upgraded designs. The key features are: wedged Ti:S crystals, spatial filtering between passes, with Brewster windows on the VSFs and image relaying from the crystal position back onto itself.

Measurements taken following commissioning have shown a significant improvement in laser contrast, a critical parameter for successful high intensity laser plasma experiments.

References

1. C Hooker *et al* – Upgrade of Astra Amplifier 3 and the Astra interlock system – CLF Annual Report 2009-10

2. K Ertel *et al* - Automatic beam alignment system for Astra, first stage – CLF Annual Report 2005-06, p187

3. N.V. Didenko, A.V. Konyashchenko, A.P. Lutsenko, S.Yu. Tenyakov - Contrast degradation in a chirped-pulse amplifier due to generation of prepulses by postpulses - *Opt. Express* **16**(5), 3178 (2008)

4. C Hooker,Y Tang,O Chekhlov, J Collier, E Divall, K Ertel,SJ Hawkes, B Parry, P.P. Rajeev - Improving coherent contrast of Petawatt laser pulses - *Opt. Express* **19**(3), 2193 (2011)